NANO LETTERS

pubs.acs.org/NanoLett Letter

Evolution of Dopant-Concentration-Induced Magnetic Exchange Interaction in Topological Insulator Thin Films

Fei Wang, Yi-Fan Zhao, Zi-Jie Yan, Deyi Zhuo, Hemian Yi, Wei Yuan, Lingjie Zhou, Weiwei Zhao, Moses H. W. Chan, and Cui-Zu Chang*

Cite This: Nano Lett. 2023, 23, 2483−2489 Read Online

ACCESS | Metrics & More | Article Recommendations | Supporting Information

ABSTRACT: To date, the quantum anomalous Hall effect has been realized in chromium (Cr)- and/or vanadium(V)-doped topological insulator $(Bi,Sb)_2Te_3$ thin films. In this work, we use molecular beam epitaxy to synthesize both V- and Cr-doped Bi_2Te_3 thin films with controlled dopant concentration. By performing magneto-transport measurements, we find that both systems show an unusual yet similar ferromagnetic response with respect to magnetic dopant concentration; specifically the Curie temperature does not increase monotonically but shows a local maximum at a critical dopant concentration. We attribute this unusual ferromagnetic response observed in Cr/V-doped Bi_2Te_3 thin films to the dopant-concentration-induced magnetic exchange interaction, which displays evolution from van Vleck-type ferromagnetism in a nontrivial magnetic topological insulator to Ruderman−Kittel−Kasuya−Yosida (RKKY)-type ferromagnetism in a trivial diluted magnetic semiconductor. Our work provides insights into the ferromagnetic properties of magnetically doped topological insulator thin films and facilitates the pursuit of high-temperature quantum anomalous Hall effect.

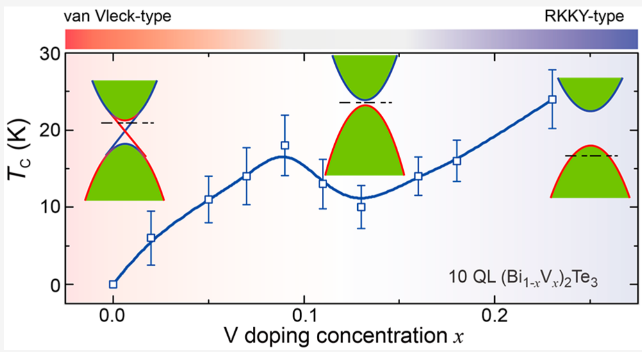

KEYWORDS: *Topological insulator, anomalous Hall effect, molecular beam epitaxy growth, thin film, magnetic exchange interaction*

The quantum anomalous Hall (QAH) effect is a topological quantum state with quantized Hall resistance and zero longitudinal resistance in the absence of external magnetic fields.[1−5] The dissipationless chiral edge states of the QAH insulators provide us with a unique opportunity to develop next-generation electronics, spintronics, and topological quantum computations with low energy consumption.[6−8] To realize a QAH insulator, the material system must possess both band topology and magnetism.[9] The most convenient approach for achieving these two essential ingredients is doping magnetic ions into a topological insulator (TI).[10,11] In magnetically doped TIs, the exchange interaction mechanism is analogous to that in conventional diluted magnetic semiconductors.[12,13] Through this approach, the QAH effect has been realized to date in two magnetically doped TI systems, i.e., Cr- and/or V-doped $(Bi,Sb)_2Te_3$ (refs 1, 10, 11, 14−16). In these two systems, Cr and V atoms are magnetic impurities that substitute the Bi/Sb sites[1,17] (Figure 1a). The formation of the ferromagnetic order breaks time-reversal symmetry and opens a magnetic exchange gap at the Dirac point of the TI. When the Fermi level is tuned into the magnetic exchange gap, the magnetic TI becomes a QAH insulator. To date, the critical temperature of the QAH state observed in these magnetically doped TI films/heterostructures is still limited to ~10 K (refs 1, 14, 18). Here the critical temperature of the QAH state is defined as that at which the ratio between the Hall and longitudinal resistances at zero magnetic field is greater than 1 (ref 1). Studies of the ferromagnetic response in Cr- and/or V-doped Bi_2Te_3 as a function of the dopant concentration can help us understand the magnetic exchange interactions and thus facilitate the exploration of higher temperature QAH insulators.

Two common magnetic exchange interactions have been proposed to be responsible for the formation of the ferromagnetic order in magnetically doped TIs. One is the van Vleck-type exchange interaction, which originates from the nonzero matrix elements of the spin operators between the bulk conduction and valence bands.[5,19] The local magnetic moments are coupled without the assistance of itinerant carriers (Figure 1b). The van Vleck-type exchange interaction relies on the strength of spin−orbit coupling (SOC) and is usually significantly enhanced by the appearance of an inverted band structure in a material. The van Vleck-type exchange

Received: September 29, 2022
Revised: March 14, 2023
Published: March 17, 2023

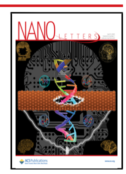

https://doi.org/10.1021/acs.nanolett.2c03827
Nano Lett. 2023, 23, 2483−2489

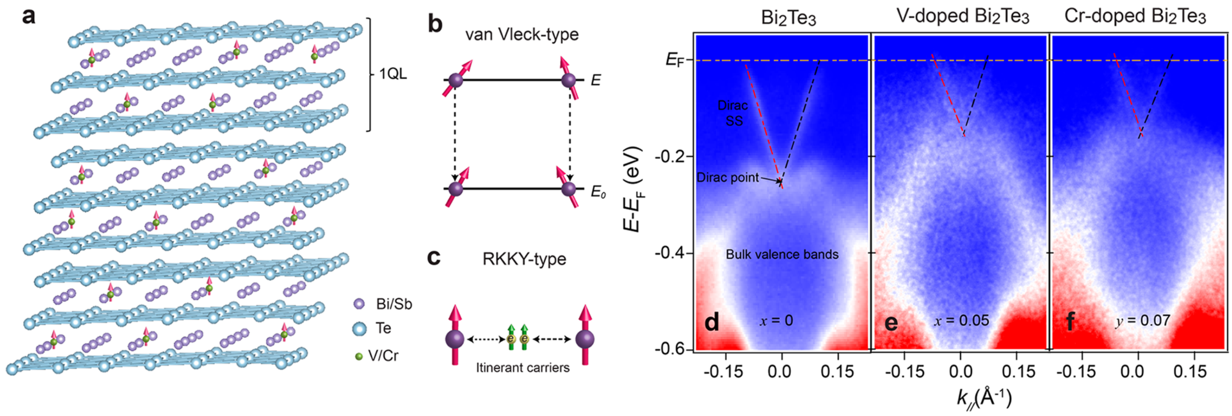

Figure 1. Two types of exchange interaction in magnetically doped TI films. (a) Schematic atomic structure of the Cr- or V-doped $(Bi,Sb)_2Te_3$ with the QAH state. Cr/V substitutes for the Bi/Sb sites. (b) van Vleck-type magnetic exchange interaction. van Vleck-type ferromagnetism is induced by the mixing of the bulk conduction and valence bands and thus can be significantly enhanced in a system with inverted band structure. It is usually insensitive to itinerant carriers. (c) RKKY-type magnetic exchange interaction. In RKKY-type ferromagnetism, local magnetic moments are coupled through itinerant carriers. (d–f) ARPES band maps of 10 QL Bi_2Te_3 (d), $(Bi_{1-x}V_x)_2Te_3$ (x = 0.05) (e), and $(Bi_{1-y}Cr_y)_2Te_3$ (y = 0.07) (f). All these samples were grown on bilayer graphene-terminated 6H-SiC(0001) substrates. All ARPES measurements were performed at room temperature. The chemical potential of Bi_2Te_3 films moves toward the Dirac point, indicating that hole-type carriers are introduced by doping Cr/V.

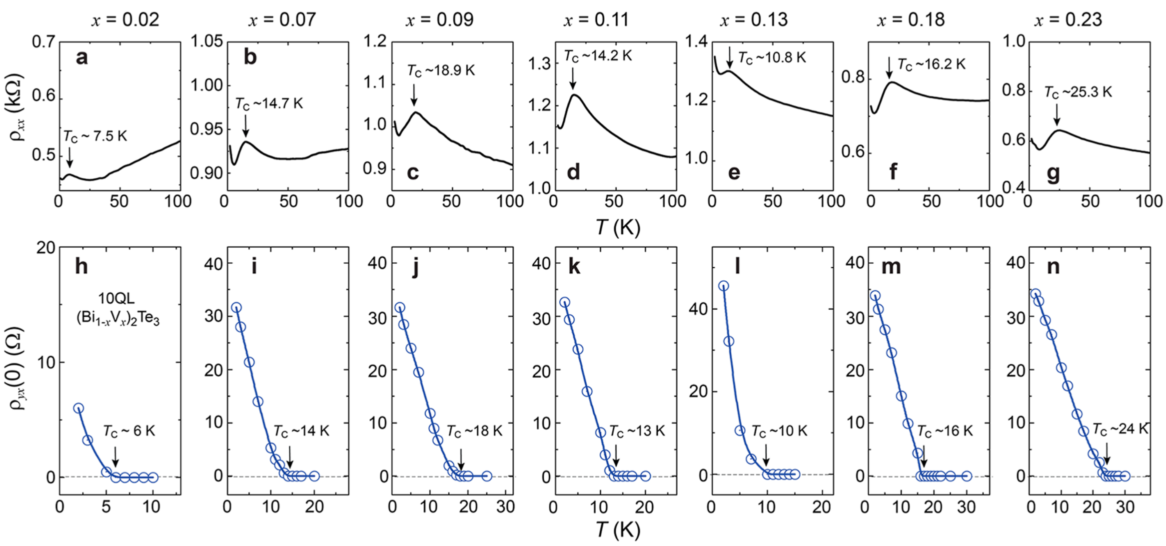

Figure 2. Transport results of 10 QL $(Bi_{1-x}V_x)_2Te_3$ films with different V dopant concentration x. (a–g) Temperature dependence of the longitudinal resistance ρ_{xx} of 10 QL $(Bi_{1-x}V_x)_2Te_3$ films: (a) x = 0.02; (b) x = 0.07; (c) x = 0.09; (d) x = 0.11; (e) x = 0.13; (f) x = 0.18; (g) x = 0.23. The hump features marked by arrows indicate the Curie temperature, T_C. (h–n) Temperature dependence of the zero magnetic field Hall resistance $\rho_{yx}(0)$ of 10 QL $(Bi_{1-x}V_x)_2Te_3$ films: (h) x = 0.02; (i) x = 0.07; (j) x = 0.09; (k) x = 0.11; (l) x = 0.13; (m) x = 0.18; (n) x = 0.23. The arrows indicate the critical temperatures at which $\rho_{yx}(0)$ is vanishing.

interaction is thought to be a prerequisite for the realization of the QAH effect in magnetically doped TIs (refs 1, 5, 10, 11, 15, 16). In addition, since the magnetically doped TI is also a special kind of diluted magnetic semiconductor, its ferromagnetic response can also be mediated through itinerant carriers by the Ruderman–Kittel–Kasuya–Yosida (RKKY) exchange interaction (Figure 1c).[12,13] In particular, when the magnetic dopant concentration is high, the SOC of a magnetically doped TI will be greatly reduced.[1,20−23] This will make the inverted band structure fade away, and the RKKY-type ferromagnetism will take over in magnetically doped TIs (refs 1, 6). In most conventional diluted magnetic semiconductors, the Curie temperature shows a monotonic increase with dopant concentration.[12,13] For a fixed dopant concentration, the ferromagnetic order can be altered by tuning the carrier density and/or electric field.[24−26]

In this work, we use molecular beam epitaxy (MBE) to synthesize V- and Cr-doped Bi_2Te_3 films with different dopant concentrations and perform *in situ* angle-resolved photoemission spectroscopy (ARPES) and *ex situ* electrical transport measurements on these films. ARPES results show that the V/Cr doping introduces hole carriers in Bi_2Te_3 films and moves their chemical potential toward the charge-neutral point. Transport results show that the Curie temperature of V/Cr-doped Bi_2Te_3 films does not increase monotonically and shows a local maximum at a critical dopant concentration. Since the Cr/V doping also reduces the SOC of Bi_2Te_3, prior studies have demonstrated that heavy Cr/V doping can drive it from a nontrivial TI to a trivial semiconductor.[1,20−23] We attribute the

https://doi.org/10.1021/acs.nanolett.2c03827
Nano Lett. 2023, 23, 2483−2489

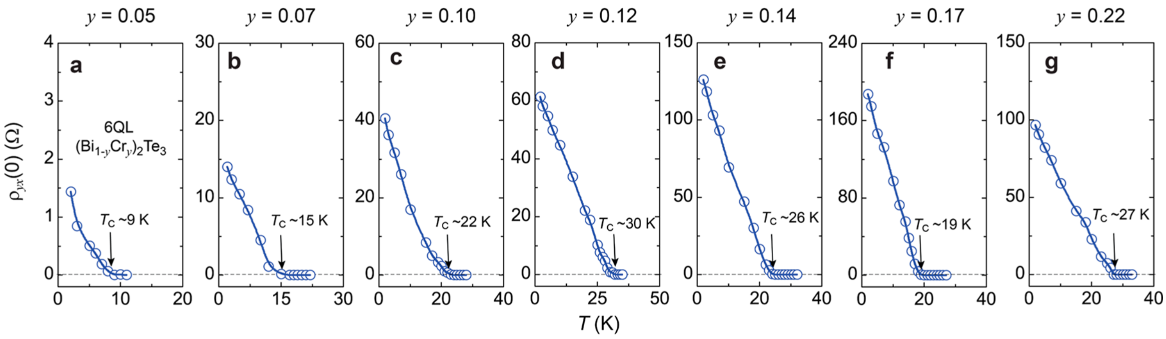

Figure 3. Transport results of 6 QL $(Bi_{1-y}Cr_y)_2Te_3$ films with different Cr dopant concentration y. (a−g) Temperature dependence of $\rho_{yx}(0)$ of 6 QL $(Bi_{1-y}Cr_y)_2Te_3$ films: (a) $y = 0.05$; (b) $y = 0.07$; (c) $y = 0.10$; (d) $y = 0.12$; (e) $y = 0.14$; (f) $y = 0.17$; (g) $y = 0.22$. The arrows indicate the critical temperatures at which $\rho_{yx}(0)$ vanishes.

unusual ferromagnetic response observed in Cr/V-doped Bi_2Te_3 thin films to an evolution of the dopant-concentration-induced magnetic exchange interaction, i.e., from the van Vleck-type ferromagnetism in a nontrivial TI that crosses over to the RKKY-type ferromagnetism in a trivial diluted magnetic semiconductor.

All $(Bi_{1-x}V_x)_2Te_3$ ($0 \leq x \leq 0.23$) and $(Bi_{1-y}Cr_y)_2Te_3$ ($0 \leq y \leq 0.29$) films used in this work were synthesized in an ultrahigh vacuum MBE chamber (Omicron Lab 10), which was connected to an ARPES chamber. Both chambers have a base vacuum of $\sim 2 \times 10^{-10}$ mbar. The Cr/V doping concentration x or y is determined by the temperature of the V/Cr source and later calibrated by inductively coupled plasma atomic emission spectroscopy (ICP-AES).[11] The *in situ* ARPES measurements were carried out using a Scientia R3000 analyzer with an unpolarized He-Iα light (~21.2 eV). Our MBE-grown V/Cr-doped Bi_2Te_3 films were characterized by atomic force microscopy (AFM), scanning tunneling microscopy (STM), X-ray diffraction (XRD), and ARPES measurements (Supplementary Figures 1 to 5). The electrical transport studies were carried out in a Physical Property Measurements System (Quantum Design, 2 K, 9 T) with the magnetic field applied perpendicular to the film plane. Six terminal mechanically defined Hall bars were used for electrical transport measurements.

We first performed ARPES measurements on undoped Bi_2Te_3 (Figure 1d), V-doped Bi_2Te_3 (Figure 1e), and Cr-doped Bi_2Te_3 (Figure 1f and Supplementary Figure 4) films with a thickness of 10 quintuple layers (QLs). For undoped Bi_2Te_3, the Dirac point is buried in the bulk valence bands. The Dirac point is located at $(E - E_F) \sim -250$ meV, reflecting the electron-type carriers.[27,28] This observation is in agreement with the negative slope of the Hall traces (Supplementary Figures 6a, 13a, and 18a). At a small V/Cr concentration in Bi_2Te_3, the gapless Dirac surface states (SSs) still appear but the chemical potential moves closer to the Dirac point. The Dirac point is located at $(E - E_F) \sim -148$ meV for the x = 0.05 sample (V doping) (Figure 1e) and ~ −142 meV for the y = 0.07 sample (Cr doping) (Figure 1f). Therefore, the V/Cr ions act as hole donors in these V/Cr-doped Bi_2Te_3 films. With further increase of the V/Cr dopant concentrations, a large number of hole carriers are introduced, which move the chemical potential across the bulk valence bands. In addition, the Dirac point is pulled out of the bulk valence bands with V/Cr doping (Figure 1e,f and Supplementary Figures 4 and 5).

Next, we carried out electrical transport measurements on both 10 QL $(Bi_{1-x}V_x)_2Te_3$ ($0 \leq x \leq 0.23$) and 6 QL $(Bi_{1-y}Cr_y)_2Te_3$ ($0 \leq y \leq 0.29$) films on heat-treated $SrTiO_3(111)$ (Figures 2 and 3). Figure 2a−g shows the temperature dependence of the longitudinal resistance ρ_{xx} of 10 QL $(Bi_{1-x}V_x)_2Te_3$ films with different V dopant concentrations x. For the x = 0.02 sample, the ρ_{xx} value decreases with decreasing T, showing metallic behavior. At $T \sim$ 7.5 K, a hump feature is observed (Figure 2a). Such behavior in the $\rho_{xx}-T$ curve of magnetic materials has been associated with the paramagnetism-to-ferromagnetism phase transition, primarily due to spin-disorder scattering.[29,30] This feature is often used to determine the magnetic ordering temperature (i.e., Curie temperature, T_C) of the ferromagnetic materials.[29,30] We next gradually increase x in V-doped Bi_2Te_3 films. For the $x \leq 0.09$ samples, the hump feature in $\rho_{xx}-T$ curves moves toward higher temperatures. The values of T_C determined by the hump feature are ~14.7 K for x = 0.07 and ~18.9 K for x = 0.09 samples, respectively (Figure 2b,c). In addition, we also find that the samples tend to show insulating behavior with increasing x in this regime, which is likely a result of the neutralization between the hole carriers introduced by the V doping and the original electron carriers in intrinsic Bi_2Te_3 (Figure 1e). With a further increase in x, the samples still show an insulating behavior, but the hump feature in $\rho_{xx}-T$ curves moves toward lower temperatures. For the x = 0.11 and x = 0.13 samples, T_C ~ 14.2 K and 10.8 K, respectively (Figures 2d,e). The lower T_C with a larger x is unusual, and unlike the behavior in most conventional diluted magnetic semiconductors.[12,13] For the $x > 0.13$ samples, the T_C value increases with increasing x again. T_C is found to be ~16.2 K for x = 0.18 and ~25.3 K for x = 0.23 samples (Figures 2f and 2g). At very low temperatures (i.e., ≲5 K), the upturn in $\rho_{xx}-T$ curves is likely a consequence of the Anderson localization-induced insulating phase (Figure 2a−g).

To validate this unusual T_C response in V-doped Bi_2Te_3 films, we performed anomalous Hall (AH) measurements on these 10 QL $(Bi_{1-x}V_x)_2Te_3$ ($0 \leq x \leq 0.23$) films under different temperatures. The T_C value can be determined by the temperature at which the AH resistance at zero magnetic field, $\rho_{yx}(0)$, vanishes. At T = 2 K, all V-doped Bi_2Te_3 samples show square-shaped hysteresis loops, demonstrating the long-range ferromagnetic order with perpendicular anisotropy (Supplementary Figures 5 and 18). These ferromagnetic hysteresis loops shrink and show a linear $\rho_{yx}-\mu_0 H$ dependence at $\sim T_C$ of the samples. We plot $\rho_{yx}(0)$ as a function of T and find that the T_C value determined by AH measurement is slightly lower than that determined by the hump feature in its corresponding $\rho_{xx}-T$ curve, but within 1.5 K (Figure 2h−n). We note that the

https://doi.org/10.1021/acs.nanolett.2c03827
Nano Lett. 2023, 23, 2483−2489

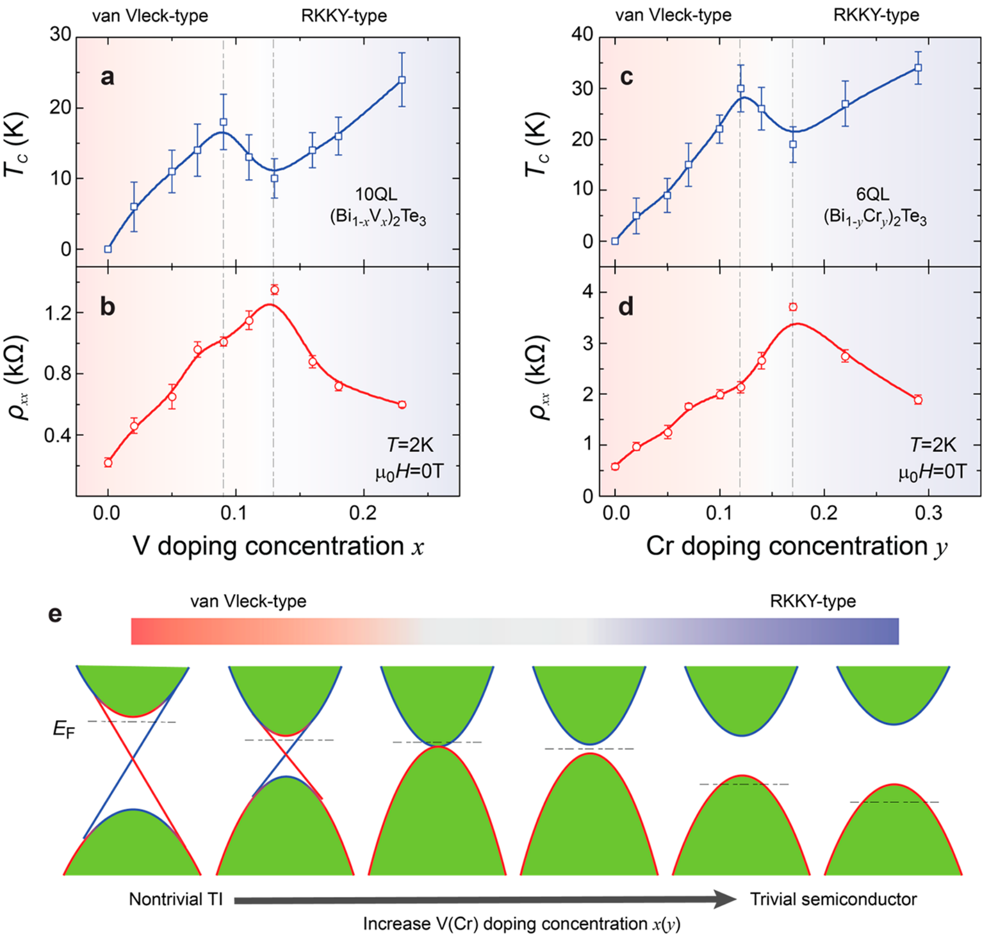

Figure 4. Evolution of dopant-concentration-induced exchange interaction in magnetically doped Bi_2Te_3. (a,b) V dopant concentration x-dependent T_C (a) and ρ_{xx} (b) of 10 QL $(Bi_{1-x}V_x)_2Te_3$ films. (c,d) Cr dopant concentration y-dependent T_C (a) and ρ_{xx} (b) of 6 QL $(Bi_{1-y}Cr_y)_2Te_3$ films. Here the T_C values are determined by the $\rho_{yx}(0)-T$ curves and the ρ_{xx} values are acquired at T = 2 K. (e) Schematics of the evolution of the electronic band structure (i.e., nontrivial to trivial) and the chemical potential position (i.e., electron- to hole-doped) with increasing V (Cr) dopant concentration x (y). The error bars in panels a and c are estimated from different T_C determinations, including the Arrott plots, the $\rho_{yx}(0)-T$ curves, the hump feature in $\rho_{xx}-T$ curves, and the disappearance of the Hall hysteresis loop in raw data. The error bars in panels b and d are estimated from the variability of the standard resistor and the accuracy of the thermometers, the voltmeters, and the current sources.

values of T_C determined by the $\rho_{yx}(0)-T$ curves also show an increase−reduce−increase behavior with a local maximum for the x = 0.09 sample (Figure 2h−n).

A similarly unusual ferromagnetic response is also observed in Cr-doped Bi_2Te_3 films. Compared to 10 QL $(Bi_{1-x}V_x)_2Te_3$($0 \leq x \leq 0.23$) films, the diminished bulk conduction contribution in 6 QL $(Bi_{1-y}Cr_y)_2Te_3$ ($0 \leq y \leq 0.29$) films smears the hump feature in their $\rho_{xx}-T$ curves (Supplementary Figure 12). Therefore, we performed AH measurements on 6 QL $(Bi_{1-y}Cr_y)_2Te_3$ ($0 \leq y \leq 0.29$) films with a narrow temperature interval ~1 K near T_C (Supplementary Figures 15 and 16). Figure 3a−g shows the temperature-dependent $\rho_{yx}(0)$ of 6 QL $(Bi_{1-y}Cr_y)_2Te_3$ films with different y. T_C determined by the temperature at which $\rho_{yx}(0)$ becomes 0 is ~9 K for y = 0.05, ~15 K for y = 0.07, ~22 K for y = 0.10, ~30 K for y = 0.12, ~26 K for y = 0.14, ~19 K for y = 0.17, and ~27 K for y = 0.22 samples. The T_C values of Cr-doped Bi_2Te_3 films also show a clear increase−reduce−increase behavior with a local maximum for the y = 0.12 sample. We note that the unusual ferromagnetic response is also observed in two more batches of 10 QL V-doped Bi_2Te_3 films on hydrogen-passivated Si(111) substrates and 5 QL Cr-doped Bi_2Te_3 films on sapphire (0001) substrates (Supplementary Figures 18 to 26).

To summarize the unusual ferromagnetic response in V/Cr-doped Bi_2Te_3 films, we plot their T_C values and ρ_{xx} values at T = 2 K as a function of magnetic dopant concentration x (y) (Figure 4a−d). As shown above, the T_C value of the V-doped Bi_2Te_3 films increases with x for $0 \leq x \leq 0.09$, decreases with x for $0.09 \leq x \leq 0.13$, and increases again with x for $x \geq 0.13$ (Figure 4a). We find that ρ_{xx} shows a peak at x = 0.13 (Figure 4b), concomitant with a local minimum of T_C. The Cr-doped Bi_2Te_3 films show similar behaviors. T_C increases with y for $0 \leq y \leq 0.12$, decreases with y for $0.12 \leq y \leq 0.17$, and increases again with y for $y \geq 0.17$(Figure 4c). Similar to the behavior of the V-doped films, ρ_{xx} shows a peak where a local minimum of T_C is found at y ~ 0.17 (Figure 4d). As noted above, the V/Cr doping inevitably introduces hole carriers into Bi_2Te_3, which consequently move the chemical potential toward the charge neutral point. Heavy V/Cr doping may make the chemical potential cross the bulk valence bands. This explains why ρ_{xx} shows a peak with varying x or y. The maximum of ρ_{xx} usually corresponds to the charge neutral point.[28,31] We note that the value of T_C increases with increasing x or y in either the van Vleck-type exchange interaction regime (i.e., $0 \leq x \leq 0.09$ and

https://doi.org/10.1021/acs.nanolett.2c03827
Nano Lett. 2023, 23, 2483−2489

$0 \le y \le 0.12$) or the RKKY-type exchange interaction regime (i.e., $0.13 \le x \le 0.23$ and $0.17 \le y \le 0.29$), probably indicating both RKKY- and van Vleck-type exchange interactions rely on the density of magnetic moments, i.e., the V/Cr doping concentration x or y in our MBE-grown $(Bi_{1-x}V_x)_2Te_3$ and $(Bi_{1-y}Cr_y)_2Te_3$ films.

Finally, we propose a phenomenological model to understand the physical origin of the unusual ferromagnetic response in V- and Cr-doped Bi_2Te_3 systems. In addition to the introduction of hole carriers, as discussed above, the V/Cr doping also reduces the SOC of Bi_2Te_3 and thus drives it from a nontrivial TI to a trivial semiconductor.[1,20−23] For low V/Cr doping, i.e., $0 \le x \le 0.09$ for V and $0 \le y \le 0.12$ for Cr, the V/Cr-doped Bi_2Te_3 film is still located in the nontrivial TI regime (Figure 4e). Its inverted band structure, particularly when its chemical potential crosses Dirac SSs, generates considerable spin susceptibility and thus the van Vleck-type exchange interaction is dominant in V/Cr-doped Bi_2Te_3 films. Therefore, the Curie temperature T_C increases because the V/Cr ions in Bi_2Te_3 introduce more electronic states in the total spin susceptibility,[5,19] while ρ_{xx} increases due to the reduced electron carrier density. We note that since the maximum of the bulk valence bands along the Γ−M direction is usually higher than the Dirac point in undoped Bi_2Te_3 (refs 27, 28, 32, 33), a minor hole carrier-mediated RKKY exchange interaction may appear when the chemical potential starts to cross the bulk valence bands.[34,35] For high V/Cr doping, i.e., $x \ge 0.13$ for V doping and $y \ge 0.17$ for Cr doping, V/Cr-doped Bi_2Te_3 film becomes a trivial semiconductor and the inverted band structure disappears (Figure 4e). The V/Cr-doped Bi_2Te_3 film is then simply a conventional diluted magnetic semiconductor, in which the van Vleck-type exchange interaction is negligible and the RKKY-type exchange interaction is dominant. We note that the van Vleck-type exchange interaction becomes negligible at the local minimum of T_C (i.e., $x \sim 0.13$ for V and $y \sim 0.17$ for Cr), which coincidentally is near the charge neutral point. This apparent coincidence might be an artifact of the limited data points in our experiments.

For the Bi_2Te_3 films with intermediate V/Cr doping, i.e., $0.09 \le x \le 0.13$ for V doping and $0.12 \le y \le 0.17$ for Cr doping, the van Vleck- and RKKY-type exchange interactions coexist and compete with each other.[34−36] In this region, an increase of V/Cr doping greatly reduces the carrier density and thus weakens the contribution of the RKKY-type exchange interaction. Moreover, the increase of V/Cr doping further reduces the SOC of Bi_2Te_3, which drives it to behave as a trivial semiconductor,[1,20−23] so the van Vleck-type exchange interaction tends to be less favored. Therefore, the total magnetic exchange interaction becomes weak and thus T_C decreases with increasing magnetic dopant concentration x or y. Based on our above analysis, the V/Cr dopant-concentration-induced quantum phase transition between nontrivial TI and trivial semiconductor phases likely occurs near $x = 0.09$ for V doping and $y = 0.12$ for Cr doping. The latter value for the Cr-doped Bi_2Te_3 system agrees well with that from our recent studies on QAH multilayer heterostructures.[22,23]

To summarize, we fabricated a series of V/Cr-doped Bi_2Te_3 films with different V/Cr dopant concentrations and found an unusual ferromagnetic response in these films, i.e., a local maximum of the Curie temperature T_C at critical V/Cr dopant concentrations. By careful analysis, we attributed this unusual ferromagnetic response in V/Cr-doped Bi_2Te_3 systems to an evolution of the magnetic exchange interaction, i.e., the crossover from van Vleck-type exchange interaction in the nontrivial TI regime to RKKY-type interaction in the trivial semiconductor regime. We conclude that the unusual ferromagnetic response of the V/Cr-doped Bi_2Te_3 films is primarily due to the two roles of the V/Cr doping: (i) it introduces a large number of hole carriers and makes the chemical potential pass through the charge neutral point and cross the bulk valence bands; (ii) it reduces the SOC of Bi_2Te_3 and drives it from a nontrivial TI to a trivial semiconductor. Our work provides insights into the magnetic exchange interactions in magnetically doped TI films/heterostructures and lays down the requirements and constraints on how to pursue the higher temperature QAH effect and other novel topological phases therein.

■ ASSOCIATED CONTENT

Supporting Information

The Supporting Information is available free of charge at https://pubs.acs.org/doi/10.1021/acs.nanolett.2c03827.

MBE growth of V/Cr-doped Bi_2Te_3 films, more sample characterizations of V/Cr-doped Bi_2Te_3 films, more transport results of 10 QL V-doped Bi_2Te_3 films on $SrTiO_3(111)$, more transport results of 6 QL Cr-doped Bi_2Te_3 films on $SrTiO_3(111)$, transport results of the second batch of on Si(111) and the other two batches of Cr-doped Bi_2Te_3 films on sapphire (0001) (PDF)

■ AUTHOR INFORMATION

Corresponding Author

Cui-Zu Chang − *Department of Physics, The Pennsylvania State University, University Park, Pennsylvania 16802, United States;* orcid.org/0000-0003-3515-2955; Email: cxc955@psu.edu

Authors

Fei Wang − *Department of Physics, The Pennsylvania State University, University Park, Pennsylvania 16802, United States; School of Material Science and Engineering, Harbin Institute of Technology, Shenzhen 518055, China*

Yi-Fan Zhao − *Department of Physics, The Pennsylvania State University, University Park, Pennsylvania 16802, United States*

Zi-Jie Yan − *Department of Physics, The Pennsylvania State University, University Park, Pennsylvania 16802, United States;* orcid.org/0000-0001-6176-319X

Deyi Zhuo − *Department of Physics, The Pennsylvania State University, University Park, Pennsylvania 16802, United States*

Hemian Yi − *Department of Physics, The Pennsylvania State University, University Park, Pennsylvania 16802, United States*

Wei Yuan − *Department of Physics, The Pennsylvania State University, University Park, Pennsylvania 16802, United States*

Lingjie Zhou − *Department of Physics, The Pennsylvania State University, University Park, Pennsylvania 16802, United States*

Weiwei Zhao − *School of Material Science and Engineering, Harbin Institute of Technology, Shenzhen 518055, China;* orcid.org/0000-0002-0373-1146

Moses H. W. Chan − *Department of Physics, The Pennsylvania State University, University Park, Pennsylvania 16802, United States*

Complete contact information is available at: https://pubs.acs.org/10.1021/acs.nanolett.2c03827

Author Contributions

C.-Z. C. conceived and designed the experiment. F. W., Y.-F. Z., Z. Y., D. Z., and L. Z. grew all V/Cr-doped Bi_2Te_3 films and carried out the PPMS transport measurements. H. Y., Z. Y., and Y. W. carried out the *in situ* ARPES measurements. F. W. and Y.-F. Z. performed the AFM and STM measurements. F. W. and C.-Z. C. analyzed the data and wrote the manuscript with input from all authors.

Notes

The authors declare no competing financial interest.

■ ACKNOWLEDGMENTS

We thank C.-X. Liu, N. Samarth, X. Wang, D. Xiao, and H. Zhang for their helpful discussions. This work is primarily supported by the NSF-CAREER award (DMR-1847811), including the MBE growth and electrical transport measurements. The ARPES measurements and sample characterization are partially supported by the AFOSR grant (FA9550-21-1-0177). C.-Z. C. also acknowledges support from the Gordon and Betty Moore Foundation's EPiQS Initiative (Grant GBMF9063 to C.-Z. C.). W. W. Z. acknowledges support from the Natural Science Foundation of China (52073075) and Shenzhen Science and Technology Program (KQTD20170809110344233).

■ REFERENCES

(1) Chang, C.-Z.; Liu, C.-X.; MacDonald, A. H. Colloquium: Quantum anomalous Hall effect. *Rev. Mod. Phys.* **2023**, *95*, 011002.
(2) Haldane, F. D. M. Model for a Quantum Hall-Effect without Landau Levels: Condensed-Matter Realization of the "Parity Anomaly". *Phys. Rev. Lett.* **1988**, *61*, 2015−2018.
(3) Liu, C. X.; Qi, X. L.; Dai, X.; Fang, Z.; Zhang, S. C. Quantum anomalous Hall effect in $Hg_{1-y}Mn_yTe$ quantum wells. *Phys. Rev. Lett.* **2008**, *101*, 146802.
(4) Qi, X. L.; Hughes, T. L.; Zhang, S. C. Topological Field Theory of Time-Reversal Invariant Insulators. *Phys. Rev. B* **2008**, *78*, 195424.
(5) Yu, R.; Zhang, W.; Zhang, H. J.; Zhang, S. C.; Dai, X.; Fang, Z. Quantized Anomalous Hall Effect in Magnetic Topological Insulators. *Science* **2010**, *329*, 61−64.
(6) Chang, C. Z.; Li, M. D. Quantum Anomalous Hall Effect in Time-Reversal-Symmetry Breaking Topological Insulators. *J. Phys. Condens. Mater.* **2016**, *28*, 123002.
(7) Weng, H. M.; Yu, R.; Hu, X.; Dai, X.; Fang, Z. Quantum Anomalous Hall Effect and Related Topological Electronic States. *Adv. Phys.* **2015**, *64*, 227−282.
(8) Tokura, Y.; Yasuda, K.; Tsukazaki, A. Magnetic topological insulators. *Nat. Rev. Phys.* **2019**, *1*, 126−143.
(9) Chang, C. Z. Marriage of topology and magnetism. *Nat. Mater.* **2020**, *19*, 484−485.
(10) Chang, C. Z.; Zhang, J. S.; Feng, X.; Shen, J.; Zhang, Z. C.; Guo, M. H.; Li, K.; Ou, Y. B.; Wei, P.; Wang, L. L.; Ji, Z. Q.; Feng, Y.; Ji, S. H.; Chen, X.; Jia, J. F.; Dai, X.; Fang, Z.; Zhang, S. C.; He, K.; Wang, Y. Y.; Lu, L.; Ma, X. C.; Xue, Q. K. Experimental Observation of the Quantum Anomalous Hall Effect in a Magnetic Topological Insulator. *Science* **2013**, *340*, 167−170.
(11) Chang, C. Z.; Zhao, W. W.; Kim, D. Y.; Zhang, H. J.; Assaf, B. A.; Heiman, D.; Zhang, S. C.; Liu, C. X.; Chan, M. H. W.; Moodera, J. S. High-Precision Realization of Robust Quantum Anomalous Hall State in a Hard Ferromagnetic Topological Insulator. *Nat. Mater.* **2015**, *14*, 473−477.
(12) Jungwirth, T.; Sinova, J.; Masek, J.; Kucera, J.; MacDonald, A. H. Theory of ferromagnetic (III,Mn)V semiconductors. *Rev. Mod. Phys.* **2006**, *78*, 809−864.
(13) Dietl, T.; Ohno, H. Dilute ferromagnetic semiconductors: Physics and spintronic structures. *Rev. Mod. Phys.* **2014**, *86*, 187.
(14) Ou, Y.; Liu, C.; Jiang, G.; Feng, Y.; Zhao, D.; Wu, W.; Wang, X. X.; Li, W.; Song, C.; Wang, L. L.; Wang, W.; Wu, W.; Wang, Y.; He, K.; Ma, X. C.; Xue, Q. K. Enhancing the Quantum Anomalous Hall Effect by Magnetic Codoping in a Topological Insulator. *Adv. Mater.* **2018**, *30*, 1703062.
(15) Checkelsky, J. G.; Yoshimi, R.; Tsukazaki, A.; Takahashi, K. S.; Kozuka, Y.; Falson, J.; Kawasaki, M.; Tokura, Y. Trajectory of the Anomalous Hall Effect towards the Quantized State in a Ferromagnetic Topological Insulator. *Nat. Phys.* **2014**, *10*, 731−736.
(16) Kou, X. F.; Guo, S. T.; Fan, Y. B.; Pan, L.; Lang, M. R.; Jiang, Y.; Shao, Q. M.; Nie, T. X.; Murata, K.; Tang, J. S.; Wang, Y.; He, L.; Lee, T. K.; Lee, W. L.; Wang, K. L. Scale-Invariant Quantum Anomalous Hall Effect in Magnetic Topological Insulators beyond the Two-Dimensional Limit. *Phys. Rev. Lett.* **2014**, *113*, 137201.
(17) Chang, C. Z.; Zhang, J. S.; Liu, M. H.; Zhang, Z. C.; Feng, X.; Li, K.; Wang, L. L.; Chen, X.; Dai, X.; Fang, Z.; Qi, X. L.; Zhang, S. C.; Wang, Y. Y.; He, K.; Ma, X. C.; Xue, Q. K. Thin Films of Magnetically Doped Topological Insulator with Carrier-Independent Long-Range Ferromagnetic Order. *Adv. Mater.* **2013**, *25*, 1065−1070.
(18) Mogi, M.; Yoshimi, R.; Tsukazaki, A.; Yasuda, K.; Kozuka, Y.; Takahashi, K. S.; Kawasaki, M.; Tokura, Y. Magnetic Modulation Doping in Topological Insulators toward Higher-Temperature Quantum Anomalous Hall Effect. *Appl. Phys. Lett.* **2015**, *107*, 182401.
(19) Li, M. D.; Chang, C. Z.; Wu, L. J.; Tao, J.; Zhao, W. W.; Chan, M. H. W.; Moodera, J. S.; Li, J.; Zhu, Y. M. Experimental Verification of the Van Vleck Nature of Long-Range Ferromagnetic Order in the Vanadium-Doped Three-Dimensional Topological Insulator Sb_2Te_3. *Phys. Rev. Lett.* **2015**, *114*, 146802.
(20) Chang, C. Z.; Tang, P. Z.; Wang, Y. L.; Feng, X.; Li, K.; Zhang, Z. C.; Wang, Y. Y.; Wang, L. L.; Chen, X.; Liu, C. X.; Duan, W. H.; He, K.; Ma, X. C.; Xue, Q. K. Chemical-Potential-Dependent Gap Opening at the Dirac Surface States of Bi_2Se_3 Induced by Aggregated Substitutional Cr Atoms. *Phys. Rev. Lett.* **2014**, *112*, 056801.
(21) Zhang, J. S.; Chang, C. Z.; Tang, P. Z.; Zhang, Z. C.; Feng, X.; Li, K.; Wang, L. L.; Chen, X.; Liu, C. X.; Duan, W. H.; He, K.; Xue, Q. K.; Ma, X. C.; Wang, Y. Y. Topology-Driven Magnetic Quantum Phase Transition in Topological Insulators. *Science* **2013**, *339*, 1582−1586.
(22) Zhao, Y. F.; Zhang, R.; Mei, R.; Zhou, L. J.; Yi, H.; Zhang, Y. Q.; Yu, J.; Xiao, R.; Wang, K.; Samarth, N.; Chan, M. H. W.; Liu, C. X.; Chang, C. Z. Tuning the Chern number in quantum anomalous Hall insulators. *Nature* **2020**, *588*, 419−423.
(23) Zhao, Y.-F.; Zhang, R.; Zhou, L.-J.; Mei, R.; Yan, Z.-J.; Chan, M. H. W.; Liu, C.-X.; Chang, C.-Z. Zero Magnetic Field Plateau Phase Transition in Higher Chern Number Quantum Anomalous Hall Insulators. *Phys. Rev. Lett.* **2022**, *128*, 216801.
(24) Ohno, H.; Chiba, D.; Matsukura, F.; Omiya, T.; Abe, E.; Dietl, T.; Ohno, Y.; Ohtani, K. Electric-Field Control of Ferromagnetism. *Nature* **2000**, *408*, 944−946.
(25) Chiba, D.; Matsukura, F.; Ohno, H. Electric-field control of ferromagnetism in (Ga,Mn)As. *Appl. Phys. Lett.* **2006**, *89*, 162505.
(26) Chiba, D.; Werpachowska, A.; Endo, M.; Nishitani, Y.; Matsukura, F.; Dietl, T.; Ohno, H. Anomalous Hall Effect in Field-Effect Structures of (Ga,Mn)As. *Phys. Rev. Lett.* **2010**, *104*, 106601.
(27) Chen, Y. L.; Analytis, J. G.; Chu, J. H.; Liu, Z. K.; Mo, S. K.; Qi, X. L.; Zhang, H. J.; Lu, D. H.; Dai, X.; Fang, Z.; Zhang, S. C.; Fisher, I. R.; Hussain, Z.; Shen, Z. X. Experimental Realization of a Three-Dimensional Topological Insulator, Bi_2Te_3. *Science* **2009**, *325*, 178−181.
(28) Zhang, J. S.; Chang, C. Z.; Zhang, Z. C.; Wen, J.; Feng, X.; Li, K.; Liu, M. H.; He, K.; Wang, L. L.; Chen, X.; Xue, Q. K.; Ma, X. C.;

Wang, Y. Y. Band Structure Engineering in $(Bi_{1-x}Sb_x)_2Te_3$ Ternary Topological Insulators. *Nat. Commun.* **2011**, *2*, 574.
(29) Zhou, Z. H.; Chien, Y. J.; Uher, C. Thin film dilute ferromagnetic semiconductors $Sb_{2-x}Cr_xTe_3$ with a Curie temperature up to 190 K. *Phys. Rev. B* **2006**, *74*, 224418.
(30) Chang, C. Z.; Liu, M. H.; Zhang, Z. C.; Wang, Y. Y.; He, K.; Xue, Q. K. Field-effect modulation of anomalous Hall effect in diluted ferromagnetic topological insulator epitaxial films. *Sci. China Phys. Mech.* **2016**, *59*, 637501.
(31) Chang, C. Z.; Zhang, Z. C.; Li, K.; Feng, X.; Zhang, J. S.; Guo, M. H.; Feng, Y.; Wang, J.; Wang, L. L.; Ma, X. C.; Chen, X.; Wang, Y. Y.; He, K.; Xue, Q. K. Simultaneous Electrical-Field-Effect Modulation of Both Top and Bottom Dirac Surface States of Epitaxial Thin Films of Three-Dimensional Topological Insulators. *Nano Lett.* **2015**, *15*, 1090−1094.
(32) Li, Y. Y.; Wang, G. A.; Zhu, X. G.; Liu, M. H.; Ye, C.; Chen, X.; Wang, Y. Y.; He, K.; Wang, L. L.; Ma, X. C.; Zhang, H. J.; Dai, X.; Fang, Z.; Xie, X. C.; Liu, Y.; Qi, X. L.; Jia, J. F.; Zhang, S. C.; Xue, Q. K. Intrinsic Topological Insulator Bi_2Te_3 Thin Films on Si and Their Thickness Limit. *Adv. Mater.* **2010**, *22*, 4002−4007.
(33) Kong, D. S.; Chen, Y. L.; Cha, J. J.; Zhang, Q. F.; Analytis, J. G.; Lai, K. J.; Liu, Z. K.; Hong, S. S.; Koski, K. J.; Mo, S. K.; Hussain, Z.; Fisher, I. R.; Shen, Z. X.; Cui, Y. Ambipolar field effect in the ternary topological insulator $(Bi_xSb_{1-x})_2Te_3$ by composition tuning. *Nat. Nanotechnol.* **2011**, *6*, 705−709.
(34) Kou, X. F.; Lang, M. R.; Fan, Y. B.; Jiang, Y.; Nie, T. X.; Zhang, J. M.; Jiang, W. J.; Wang, Y.; Yao, Y. G.; He, L.; Wang, K. L. Interplay between Different Magnetisms in Cr-Doped Topological Insulators. *ACS Nano* **2013**, *7*, 9205−9212.
(35) Zhang, Z. C.; Feng, X.; Guo, M. H.; Li, K.; Zhang, J. S.; Ou, Y. B.; Feng, Y.; Wang, L. L.; Chen, X.; He, K.; Ma, X. C.; Xue, Q. K.; Wang, Y. Y. Electrically Tuned Magnetic Order and Magneto-resistance in a Topological Insulator. *Nat. Commun.* **2014**, *5*, 4915.
(36) Kim, J.; Jhi, S. H.; MacDonald, A. H.; Wu, R. Q. Ordering mechanism and quantum anomalous Hall effect of magnetically doped topological insulators. *Phys. Rev. B* **2017**, *96*, 140410.

https://doi.org/10.1021/acs.nanolett.2c03827
Nano Lett. 2023, 23, 2483−2489